PNAS RESEARCH ARTICLE | MICROBIOLOGY

Structural signatures of *Escherichia coli* chemoreceptor signaling states revealed by cellular crosslinking

Caralyn E. Flack[a] and John S. Parkinson[a,1]

Edited by Bonnie Bassler, Princeton University, Princeton, NJ; received March 8, 2022; accepted May 11, 2022

The chemotaxis machinery of *Escherichia coli* has served as a model for exploring the molecular signaling mechanisms of transmembrane chemoreceptors known as methyl-accepting chemotaxis proteins (MCPs). Yet, fundamental questions about signal transmission through MCP molecules remain unanswered. Our work with the *E. coli* serine chemoreceptor Tsr has developed in vivo reporters that distinguish kinase-OFF and kinase-ON structures in the cytoplasmic methylation helix (MH) cap, which receives stimulus signals from an adjoining, membrane-proximal histidine kinase, adenylyl cyclases, MCPs, and phosphatases (HAMP) domain. The cytoplasmic helices of the Tsr homodimer interact mainly through packing interactions of hydrophobic residues at *a* and *d* heptad positions. We investigated the in vivo crosslinking properties of Tsr molecules bearing cysteine replacements at functionally tolerant *g* heptad positions in the N-terminal and C-terminal cap helices. Upon treatment of cells with bismaleimidoethane (BMOE), a bifunctional thiol-reagent, Tsr-G273C/Q504C readily formed a doubly crosslinked product in the presence of serine but not in its absence. Moreover, a serine stimulus combined with BMOE treatment during in vivo Förster resonance energy transfer–based kinase assays locked Tsr-G273C/Q504C in kinase-OFF output. An OFF-shifting lesion in MH1 (D269P) promoted the formation of the doubly crosslinked species in the absence of serine, whereas an ON-shifting lesion (G268P) suppressed the formation of the doubly crosslinked species. Tsr-G273C/Q504C also showed output-dependent crosslinking patterns in combination with ON-shifting and OFF-shifting adaptational modifications. Our results are consistent with a helix breathing-axial rotation-bundle repacking signaling mechanism and imply that in vivo crosslinking tools could serve to probe helix-packing transitions and their output consequences in other regions of the receptor molecule.

bacterial chemotaxis | signal transduction | four-helix bundle

Significance

The conformational changes that accompany signaling events in transmembrane chemoreceptors are difficult to follow with structural methods that cannot replicate the native cellular environment. We developed in vivo cysteine crosslinking reporters of the *Escherichia coli* serine chemoreceptor Tsr that distinguished its signal-state structures. Crosslinking treatment of cells containing marked receptors produced substantial amounts of crosslinked forms in the presence of serine but not in its absence. Moreover, crosslink formation during in vivo signaling assays locked receptor output in the serine-induced output state. Output-shifting mutational changes or adaptational modifications also altered crosslinking patterns of Tsr reporters. These in vivo crosslinking assays probably detect transitions in helix-packing arrangements of the receptor molecule and may provide generally applicable tools for receptor signaling studies.

Motile bacteria efficiently move toward favorable chemical environments and away from inhospitable ones. Such behaviors play important roles in establishing beneficial host symbioses and pathogenic infections, highlighting the value of a detailed mechanistic understanding of bacterial chemotaxis machinery (1–4). The chemotaxis system of *Escherichia coli* has been most extensively studied and serves as the paradigm molecular model (5–7). The principal chemoeffector sensors in *E. coli* are transmembrane receptors known as methyl-accepting chemotaxis proteins (MCPs). MCP homodimers form mixed trimers-of-dimers that recruit two cytoplasmic signaling partners, namely, a signaling autokinase (CheA) and a scaffolding protein (CheW) that couples CheA activity to receptor control. The minimal signaling unit or core complex is comprised of two receptor trimers of dimers, one CheA homodimer and two CheW proteins (8). Core complexes organize into extended hexagonal arrays that monitor the cell's chemical environment with high detection sensitivity and response cooperativity (9).

In the absence of an attractant signal, CheA autophosphorylates and donates its phosphoryl groups to the CheY response regulator. Phospho-CheY interacts with the base of the rotary flagellar motor to trigger random changes in swimming direction. Binding of an attractant chemical to the external periplasmic domain of a chemoreceptor suppresses CheA activity at the receptor's cytoplasmic tip (Fig. 1*A*), which promotes forward, up-gradient swimming because directional changes subside rapidly due to action of a dedicated phospho-CheY phosphatase (CheZ). Attractant stimuli also modulate slower covalent modifications of the chemoreceptors that serve as a memory of the recently encountered chemical past. By comparing the ligand occupancy and modification states of its chemoreceptors, the cell is able to assess its direction of travel in a chemical gradient and respond accordingly. The following two MCP-specific enzymes control receptor modification state: CheR, a glutamyl methyltransferase, and CheB, a glutamyl methylesterase and glutaminyl deamidase. CheR and CheB act at conserved adaptation sites in the receptor cytoplasmic domain (Fig. 1). Attractant-stimulated

Author affiliations: [a]School of Biological Sciences, University of Utah, Salt Lake City, UT 84112

Author contributions: C.E.F. and J.S.P. designed research; C.E.F. performed research; C.E.F. and J.S.P. analyzed data; and C.E.F. and J.S.P. wrote the paper.

The authors declare no competing interest.

This article is a PNAS Direct Submission.

[1]To whom correspondence may be addressed. Email: parkinson@biology.utah.edu.

This article contains supporting information online at http://www.pnas.org/lookup/suppl/doi:10.1073/pnas.2204161119/-/DCSupplemental.

Published July 5, 2022.

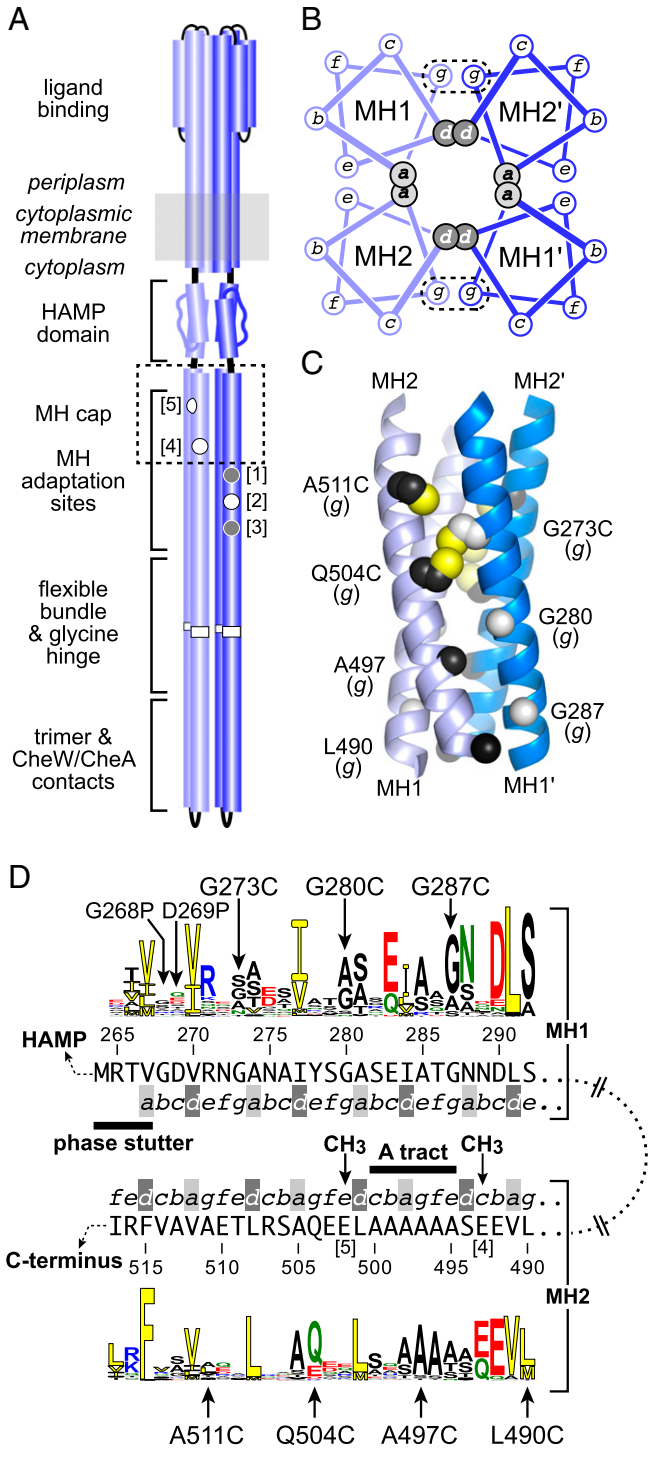

Fig. 1. Structural features of the Tsr MH cap. (*A*) Topology and signaling elements of a Tsr homodimer. Subunits are depicted in light and dark blue; cylinders represent α-helices. Circles ([1] to [5]) indicate substrate residues (glutaminyl, gray; glutamyl, white) for the adaptation enzymes CheB and CheR. (*B*) Helical wheel diagrams of a possible packing arrangement for the antiparallel, four-helix coiled-coil MH cap bundle. Heptad positions *a* to *g* denote the residues in two helical turns, as follows: *a* and *d* are typically hydrophobic packing residues; positions *e* and *g* are residues at the bundle edges; and positions *b*, *c*, and *f* are fully solvent-exposed residues. The close proximity of residues at heptad *g* positions on MH1 and MH2' (or MH2 and MH1') suggested promising targets for cysteine-directed crosslinking studies. (*C*) Structural model of the Tsr MH cap (23). Single white (MH1) and black (MH2) spheres show the α-carbon of some *g* position sidechains; residues G273, Q504, and A511 are shown as cysteines with sulfhydryl groups colored yellow. (*D*) Sequence conservation Weblogo (59) of the MH cap region in 2,428 nonredundant members of the 36H class of MCP chemoreceptors (10, 49, 60). Tsr residue numbers and amino acids are listed just below (MH1) or above (MH2) their sequence logo. Residue heptads are shown with packing positions *a* and *d* shaded as in *B*. Other relevant features include an alanine tract, flanked by modification sites [4] and [5]; a four-residue phase stutter at the junction between the HAMP AS2 helix and the MH1 helix; and the positions and residue changes of Tsr MH cap mutants used in this study.

receptors in the kinase-OFF output state are good substrates for CheR; ligand-free receptors in a kinase-ON output state are good substrates for CheB. Thus, as the cell swims about in a chemical gradient, sensed chemoeffectors modulate the relative activities of the CheR and CheB adaptation enzymes to bring about net changes in receptor modification state, ensuring persistent travel in favorable directions as chemoeffector levels fluctuate.

Although the *E. coli* chemotaxis system is well-studied, fundamental questions remain about the mechanism(s) of signal propagation through chemoreceptor molecules. The MCP superfamily is defined by a highly conserved cytoplasmic domain that can operate with a wide array of periplasmic sensing domains (10). The two high-abundance *E. coli* receptors, namely, Tsr (serine sensor) and Tar (aspartate and maltose sensor), have predominantly α-helical secondary structures organized into a ligand binding domain; a four-helix transmembrane bundle; a parallel coiled-coil HAMP (histidine kinase, adenylyl cyclases, MCPs, and phosphatases) domain; and an extended antiparallel four-helix coiled-coil domain comprising a methylation helix (MH) bundle with adaptation sites, a flexible bundle, and a membrane-distal protein interaction hairpin tip (Fig. 1*A*). The HAMP-proximal cap (Fig. 1*A*) of the MH bundle receives conformational input from HAMP and relays it to the adaptation sites, flexible region, and hairpin tip. Achieving a clear mechanistic understanding of how HAMP transmits attractant-induced signals through the MH cap and bundle is currently the focus of many research groups.

Prevailing models posit that adjacent signaling elements in the MCP cytoplasmic domain couple in conformational opposition such that enhanced stability in one induces more dynamic behavior of its adjoining neighbors. Dynamics-based mechanisms of this sort could allow small input energies from ligand binding to propagate over the ∼200-Å distance to the CheA-controlling hairpin tip (5, 6, 11–13). Experiments that have been used to investigate structural and dynamic changes in the chemoreceptor signaling domain include hydrogen-deuterium exchange mass spectrometry (14–16), solid-state NMR (17, 18), and tagging receptor molecules with electron paramagnetic resonance (EPR) reporters (19–21) or reporters for measuring Förster resonance energy transfer (FRET) interactions (22). Those studies were exclusively done in vitro using full-length Tar or soluble Tar chimeras or fragments. Although that work has documented dynamics changes in different helices or segments of the receptor cytoplasmic domain, the mechanistic basis for those changes is not yet apparent. What is needed is a way to detect, ideally in vivo, stimulus-dependent changes in helix-packing arrangements that might influence receptor conformational dynamics. This report describes a promising approach toward that goal.

Our study employed in vivo crosslinking of engineered cysteine residues at the HAMP-MH bundle junction in full-length Tsr, the *E. coli* serine chemoreceptor. The N-terminal (MH1) and C-terminal (MH2) helices of the Tsr bundle cap probably form a dynamic four-helix bundle through hydrophobic packing interactions of heptad *a* and *d* residues (Fig. 1*B*). A Tsr structural model (23) indicated that cysteines at heptad *g* positions in the MH1 and MH2 cap helices should be close enough to crosslink,

either through disulfide bonds or with a longer bifunctional thiol reagent (Fig. 1*C*). In addition, the cap *g*-position residues are not as highly conserved as the hydrophobic *a* and *d* residues, suggesting that they might tolerate cysteine replacements with little effect on Tsr signaling performance (Fig. 1*D*). Accordingly, we surveyed cysteine reporters at *g*-heptad positions for significant stimulus- or output-dependent changes in crosslinking behavior. Our results indicate that transitions between kinase-ON and kinase-OFF output states in the Tsr MH cap entail changes in helix-packing arrangements that could in turn reflect the dynamic structural properties seen in previous in vitro receptor studies.

Results

Crosslinking at *g* Heptad Residues in the MH Bundle Cap. The MH1 and MH2 helices of the MH cap engage in antiparallel coiled-coil packing interactions through hydrophobic residues at *a* and *d* heptad positions (Fig. 1*B*). Residues at *e*- and *g*-positions border the helix-packing residues (Fig. 1*B*) but are less highly conserved (Fig. 1*D*). Thus, cysteine replacements at those edge positions might not disrupt hydrophobic packing of the MH cap bundle and could report on changes in helix-packing arrangements. In this study, we exploited *g*-position MH cap residues because crosslinking between cysteines at *g* sites in the MH1 and MH2 helices should produce easily detected dimeric crosslinking products (Fig. 1*B*).

We created Tsr single-cysteine replacements at *g* sites in MH1 (G273C, G280C, G287C) and MH2 (L490C, A497C, Q504C, A511C) (Fig. 1*D*) in compatible expression plasmids pRR53 and pPA114 (24). We then constructed five MH1/MH2 double reporters chosen for the probable proximity of their sites in adjacent packing layers of the MH cap bundle. For example, G273C (MH1) was combined with A511C or Q504C (MH2) (Fig. 1 *C* and *D*). Two additional double cysteine reporters were constructed at nonadjacent sites for control purposes (G273C/A497C and G273C/L490C). All single- and double-mutant receptors exhibited steady-state intracellular amounts within twofold of wild-type Tsr (*SI Appendix*, Table S1). Moreover, all single cysteine mutant receptors, one of the adjacent double reporters (G273C/Q504C), and both of the nonadjacent double reporters exhibited fully wild-type chemotaxis performance in soft agar assays (*SI Appendix*, Fig. S1*A*).

Plasmids carrying single- or double-reporter constructs were expressed in host strain UU2610 (*SI Appendix*, Table S2), which lacks all chromosomally encoded MCPs and the CheR and CheB adaptation enzymes, thus ensuring a homogeneous modification state for the plasmid-encoded receptor molecules. The cells were treated with bismaleimidoethane (BMOE), a bifunctional thiol-reactive crosslinking reagent that readily permeates *E. coli*. Cell lysates were evaluated by sodium dodecyl sulfate–polyacrylamide gel electrophoresis (SDS-PAGE) and anti-Tsr immunoblotting. Receptors with adjacent Cys reporter pairs exhibited two prominent dimer-sized bands that were not present in any of the single-cysteine samples, which showed only minor amounts of discrete dimer-sized products (*SI Appendix*, Fig. S1*B*). We designate these crosslinked species by the helices involved. MH1-Cys reporters can only form 1-1' products; MH2-Cys reporters can only form 2-2' products. The bands unique to the double-Cys receptors should be subunits joined by one or two heterologous crosslinks (see Fig. 1 *B* and *C*). Coexpression of two single-cysteine receptors in cells (G273C+Q504C or G273C+A497C) produced, in addition to 1-1' and 2-2' products, the upper of those prominent bands, which must be the 1-2' species (*SI Appendix*, Fig. S2 *A* and *C*). The lower prominent band in double-Cys reporter samples is, therefore, the doubly linked species 1-2'/1'-2. Formation of that crosslinking product depends on the spatial proximity of the cysteine sites because the nonadjacent G273C/A497C and G273C/L490C reporter pairs produced minimal amounts of 1-2' crosslinking product and none of the doubly linked form (*SI Appendix*, Figs. S1*C* and S2 *A–C*). Taken together, these initial findings suggested that the MH cap retains a substantial coiled-coil structure in native receptor signaling complexes. To pursue this lead, we focused on the G273C/Q504C adjacent reporter pair, which produced robust crosslinking signals and supported wild-type chemotaxis performance. For convenience, we designate this double reporter receptor as Tsr^{gg}.

BMOE-Induced Tsr^{gg} Crosslinks Are Not Disulfide Bonds. BMOE has an 8 Å spacer length, whereas disulfide bond lengths are 2 to 3 Å. We found that Cu^{++}-phenanthroline, which promotes cellular disulfide bond formation, also crosslinked Tsr^{gg} molecules (*SI Appendix*, Fig. S2*C*), indicating that the reporter cysteines in Tsr^{gg} dimers can achieve the close proximity required for disulfide bond formation. All of the Cu^{++}-phenanthroline-induced Tsr^{gg} crosslinking products reverted to monomer size upon reduction with 175 mM dithiothreitol (DTT), confirming that they were linked exclusively by S-S bonds (*SI Appendix*, Fig. S2*D*). In contrast, BMOE crosslinking products of both Tsr^{gg} and the nonadjacent G273C/A497C cysteine pair were unaffected by DTT treatment (*SI Appendix*, Fig. S2*B*). We conclude that BMOE links Tsr^{gg} subunits directly rather than through disulfide bond formation.

Tsr^{gg} Crosslinking Is Attractant Dependent. In initial tests, cells treated with serine, the principal attractant chemoeffector for Tsr, produced greater amounts of Tsr^{gg} crosslinking products than untreated cells (*SI Appendix*, Fig. S1*C*). Tsr^{gg} crosslinking time courses revealed substantial rate differences in the presence and absence of a serine stimulus. Without serine, the 1-2' and 1-2'/1'-2 products slowly increased over 120 s, but the majority of Tsr^{gg} subunits remained as monomers (Fig. 2*A*). In the presence of serine, the monomer fraction dwindled rapidly, with early accumulation of the 1-2' product. At later times, the 1-2'/1'-2 product predominated (Fig. 2*A*). A stacked bar graph shows the relative amounts of each species over the time course (Fig. 2*B*). With serine, nearly all (>96%) of the Tsr^{gg} subunits were in a crosslinked form by 2 min. This extent of crosslinking was not observed in either of the single cysteine receptors (G273C or Q504C) even after 10 min (*SI Appendix*, Fig. S3 *A–D*). In a longer Tsr^{gg} time course, the 1-2'/1'-2 species reached its maximal amount (~20%) by 1.5 min in the absence of serine (*SI Appendix*, Fig. S3 *E* and *F*). In the presence of serine, Tsr^{gg} showed faster crosslinking kinetics and by 1.5 min had reached a higher maximal amount (~60%) of the 1-2'/1'-2 species (*SI Appendix*, Fig. S3 *E* and *F*).

To confirm that the serine effects on Tsr^{gg} crosslinking were due to its chemoeffector action, we introduced a serine binding-site lesion into the periplasmic domain of the Tsr^{gg} receptor. The R69E replacement in the binding pocket substantially reduces the affinity of Tsr for serine (*SI Appendix*, Fig. S4*A*) (25, 26). Crosslinking dose responses showed almost complete crosslinking of Tsr^{gg} at 1 mM serine, whereas its R69E derivative required 10 mM serine for complete crosslinking (*SI Appendix*, Fig. S4*B*), roughly a 10-fold reduction in serine sensitivity. This result demonstrates that the crosslinking changes observed in the presence of serine are due to its binding interaction with the periplasmic ligand binding domain of

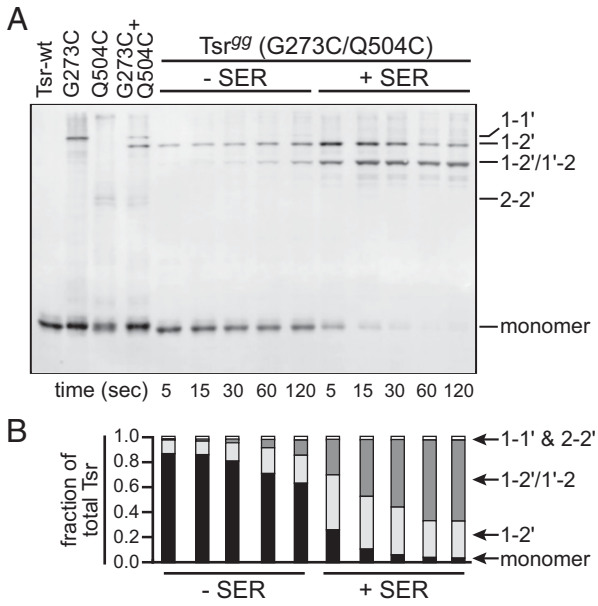

Fig. 2. Tsr^{gg} (G273C/Q504C) crosslinking in the presence and absence of the attractant serine. (*A*) Crosslinking time course. Plasmid-encoded Tsr^{gg} proteins were expressed in host strain UU2610 (ΔcheRB), and cells were treated with BMOE for the indicated times either in the presence or absence of serine. Whole-cell lysates were analyzed by SDS-PAGE, and Tsr bands were identified by immunoblotting. Single-cysteine controls in the left lanes define positions for the 1-1' and 2-2' crosslinked species; the G273C+Q504C coexpression sample defines the 1-2' crosslinked species. The doubly crosslinked 1-2'/1'-2 species is present only in the Tsr^{gg} (G273C/Q504C) double-cysteine reporter samples. SER, serine. (*B*) Quantification of the crosslinking time courses.

Tsr^{gg} and, therefore, that an attractant stimulus triggers conformational changes in the MH cap region that are detectable with Tsr^{gg} crosslinking assays.

Ligand-Dependent Tsr^{gg} Crosslinking Occurs within a Dimer; Core Signaling Complexes Are Unnecessary. Chemoreceptors alone can assemble trimers of dimers (27, 28) but require their CheA and CheW partners to form core signaling units (8). In vitro studies have shown that receptor molecules are more mobile in the absence of bound CheA/CheW (14, 29). By contrast, the formation of core signaling units enhances the propagation of conformational changes between the sensory adaptation sites and the periplasmic sensing domain of Tsr (30) and Tar (31) receptors. To test whether core unit assembly influenced Tsr^{gg} crosslinking patterns, we compared BMOE crosslinking products from strains UU2610 (*cheA*$^{+}$*W*$^{+}$) and UU2806 (Δ*cheAW*). The crosslinking patterns were quite similar; both strains exhibited serine-enhanced formation of the 1-2'/1'-2 species in comparable amounts (*SI Appendix*, Fig. S5*A*). This result implies that the serine-induced conformational changes that influence crosslinking can propagate through Tsr^{gg} molecules that are not organized into core signaling units. It seems unlikely that trimer-of-dimers organization is necessary for the serine crosslinking effect because attractant stimuli clearly influence the CheR/CheB substrate properties of isolated receptor dimers in nanodiscs (32).

The absence of core units could conceivably create opportunities for crosslinking between Tsr^{gg} subunits in different dimers. We explored this possibility with a D36C reporter site that resides at the membrane-proximal dimer interface in the receptor periplasmic domain. This Tsr reporter (and its Tar counterpart) forms a disulfide crosslink between the two subunits within a dimer and has been used to stabilize receptor homodimers for structural studies and to test for higher-order crosslinking products (29, 33–35). Although Tsr-D36C alone supported chemotaxis, it did not in combination with single- or double-cysteine MH cap reporters (*SI Appendix*, Fig. S5*B*). Nevertheless, the D36C/MH cap reporters did not produce crosslinking products larger than dimers in either the Δ*cheAW* (*SI Appendix*, Fig. S5*C*) or *cheA*$^{+}$*W*$^{+}$ strain (*SI Appendix*, Fig. S5*D*). Most crosslinking bands were little changed by DTT treatment with the exception of some preexisting disulfide-bonded products in the D36C constructs (*SI Appendix*, Fig. S5 *C* and *D*). We conclude that in both the presence and absence of core units, Tsr^{gg} crosslinking occurs within the receptor dimer. The nonadjacent reporter pair G273C/A476C showed similar behavior (*SI Appendix*, Fig. S5*D*).

ON- and OFF-Shifting Lesions Have Opposing Effects on Tsr^{gg} Crosslinking Patterns. Because serine stimuli shift Tsr output toward the kinase-OFF state (30, 36), serine-induced accumulation of the 1-2'/1'-2 Tsr^{gg} crosslinking product presumably reflects the OFF-state structure of the MH cap. If so, then OFF-shifting mutational changes should also promote Tsr^{gg} crosslinks. Conversely, ON-shifting structural changes should disfavor Tsr^{gg} crosslinks. We tested this prediction with MH1 proline replacements that lock wild-type Tsr into a kinase-ON (G268P) or kinase-OFF (D269P) output state. We documented the output behaviors of these mutant receptors in two ways, as follows: by examining their substrate properties for the CheR and CheB adaptation enzymes and by measuring the in vivo kinase activities of their signaling complexes.

Receptors in the kinase-OFF state are typically good substrates for CheR and poor substrates for CheB, whereas kinase-ON receptors are good substrates for CheB and poor substrates for CheR (6, 37, 38). The G268P receptor was modified well in CheB-containing cells and poorly by CheR-containing cells, consistent with an ON-shifted output (Fig. 3*A*). By contrast, the D269P receptor was modified well in CheR^{+} hosts but poorly in CheB^{+} hosts, indicating OFF-shifted behavior (Fig. 3*A*). In vivo FRET kinase assays confirmed these output assignments (Fig. 3*B*). This assay follows the CheA-dependent production of phospho-CheY through a FRET interaction between YFP-tagged CheY and CFP-tagged CheZ, its phosphatase partner (36, 39). The YFP/CFP signal reflects CheA activity because autophosphorylation of CheA is the rate-limiting step in the phosphorylation of CheY. In this assay, Tsr-G268P showed no FRET change in response to a 10 mM serine stimulus, but KCN treatment, which can stop CheA autophosphorylation by depleting the cellular ATP pool, produced a drop in the YFP/CFP signal, which is indicative of locked-ON kinase activity (Fig. 3*B*) (40). Tsr-D269P also failed to respond to 10 mM serine, but it was also unable to respond to KCN, consistent with a locked-OFF output (Fig. 3*B*). The inability of G268P and D269P derivatives of wild-type Tsr to respond to serine in FRET kinase assays is mirrored in their nonchemotactic behaviors in soft agar plates (*SI Appendix*, Fig. S6 *A* and *B*).

G268P and D269P derivatives of Tsr^{gg} exhibited different crosslinking time course behaviors (*SI Appendix*, Fig. S6 *C* and *D*). Even at the shortest time point, Tsr^{gg}-D269P showed substantial crosslinking in the absence of serine, although serine further increased the amount of crosslinked products (*SI Appendix*, Fig. S6*D*). Overall, Tsr^{gg}-G268P exhibited slower crosslinking rates, particularly in the absence of serine (*SI Appendix*, Fig. S6*C*). These findings strengthen the idea that the 1-2'/1'-2 crosslinking product reflects the kinase-OFF structure of the MH cap, regardless of whether the OFF state is induced by an attractant stimulus or a structure-perturbing lesion.

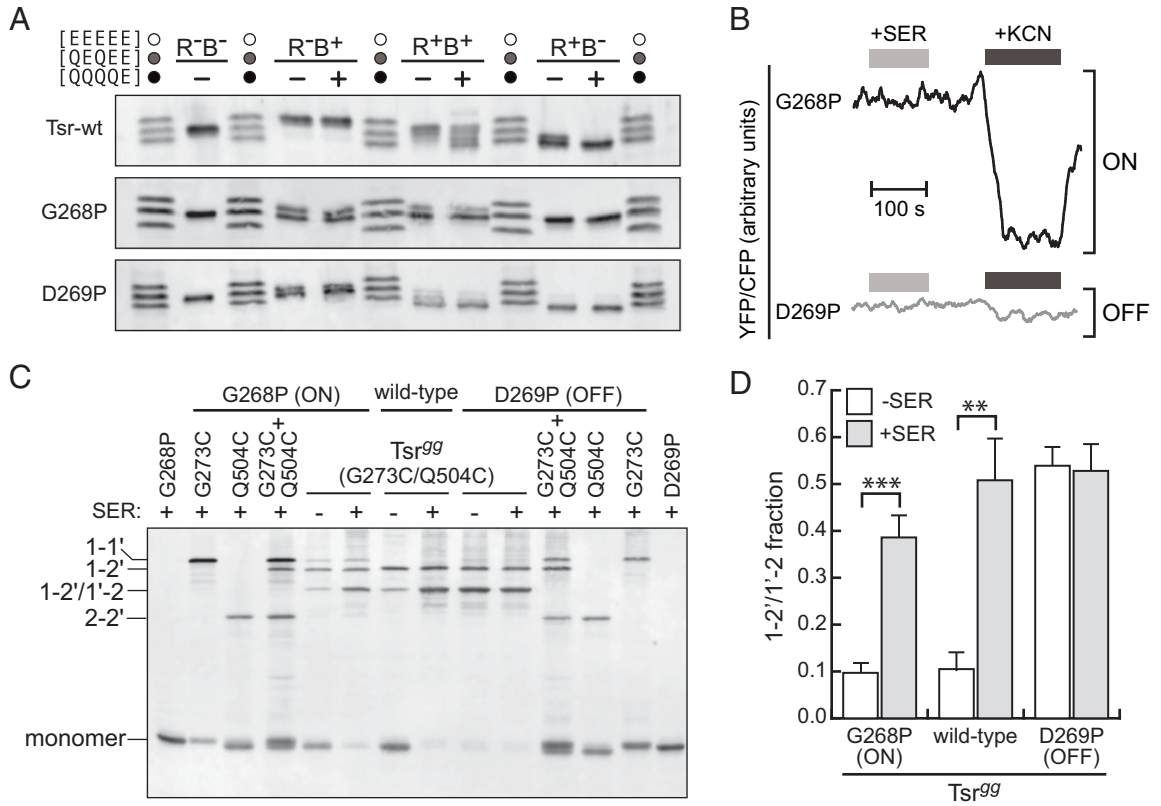

Fig. 3. Modification, signaling, and crosslinking behaviors of G268P and D269P receptors. (*A*) Adaptational modification patterns. Mutant proteins were expressed in hosts containing CheR only (R^+B^-), CheB only (R^-B^+), both (R^+B^+), or neither enzyme (R^-B^-) and analyzed with SDS-PAGE immunoblots. CheR-mediated methylation shifts bands downward; CheB-mediated deamidation or demethylation shifts bands upward. Lane symbols: circles indicate a mixture of three Tsr mobility standards [EEEEE] (white), [QEQEE] (gray), and [QQQQE] (black); -, no serine; +, serine. (*B*) Kinase CheA activities produced by Tsr^{gg}-G268P and Tsr^{gg}-D269P receptors. Signaling properties of the mutant receptors were characterized with in vivo FRET kinase assays in receptorless host strain UU2567. FRET signals (YFP/CFP) for the two mutants are shown at the same scale. Neither responded to 10 mM serine (+SER), but upon treatment with 3 mM KCN, the G268P cells showed a FRET drop, indicative of kinase activity (40). (*C*) SDS-PAGE immunoblot of crosslinked Tsr^{gg}-G268P or Tsr^{gg}-D269P. BMOE crosslinking was performed for 1.5 min in the presence or absence of serine. (*D*) Quantification of crosslinking results from three independent replicates of the experiment in *C*. Histogram bars show the mean ± SD fraction of doubly crosslinked Tsr subunits in the samples. Asterisks denote a significant difference based on a *P* value of <0.001 (***) or <0.01 (**).

We chose a 1.5-min reaction time (see *SI Appendix*, Fig. S6 *C* and *D*) for additional experimental replicates to quantify these crosslinking behaviors, following production of the 1-2'/1'-2 species (Fig. 3 *C* and *D*). Both with and without serine, Tsr^{gg}- D269P crosslinked to the same high extent as did Tsr^{gg} in the presence of serine, consistent with D269P creating a kinase-OFF structural condition. Tsr^{gg} and Tsr^{gg}-G268P crosslinked to a similar low extent in the absence of serine, consistent with G268P creating a kinase-ON output state. A serine stimulus enhanced crosslinking of Tsr^{gg}-G268P (Fig. 3*D*), indicating that its ON-shifted MH cap can still undergo attractant-induced structural changes.

Adaptational Modification State Also Influences Tsr^{gg} Crosslinking Behavior. The high-abundance *E. coli* chemoreceptors Tsr and Tar have four methylation sites in common; Tsr has a fifth site (E502) not used in Tar (41, 42). Wild-type Tsr subunits have a [QEQEE] residue pattern at their five sites, with the Q sites mimicking the signaling properties of methylated E sites. Tsr [EEEEE] has strongly OFF-shifted signaling behavior, whereas Tsr [QQQQE] has strongly ON-shifted signaling behavior (*SI Appendix*, Table S3). We examined crosslinking patterns of these Tsr^{gg} derivatives in UU2610, which lacks both CheR and CheB and so cannot alter the modification patterns. In a host with the adaptation enzymes, both Tsr^{gg} derivatives supported wild-type chemotaxis performance (*SI Appendix*, Fig. S7 *A* and *B*). In BMOE crosslinking time courses, Tsr^{gg} [EEEEE], the OFF-shifted receptor, crosslinked more extensively than its ON-shifted [QQQQE] counterpart in the absence of serine (*SI Appendix*, Fig. S7 *C* and *D*). Both receptors showed extensive crosslinking in the presence of serine, but Tsr^{gg} [EEEEE] had a faster rate (*SI Appendix*, Fig. S7 *C* and *D*), behavior that is again consistent with its OFF-shifted output state.

We chose a 1.5-min reaction time (*SI Appendix*, Fig. S7 *C* and *D*) for additional experimental replicates to quantify these crosslinking behaviors (Fig. 4*A*). In the absence of serine, the three modification states of Tsr^{gg} showed significantly different amounts of the 1-2'/1'-2 crosslinking product (Fig. 4*B*). The OFF-shifted [EEEEE] derivative had the highest amount, and the ON-shifted [QQQQE] derivative had the lowest amount. These results demonstrate that in the absence of serine, the Tsr^{gg} reporter detected structural differences between the three modification states that paralleled their signal output properties. Moreover, all three receptor forms showed extremely significant crosslinking increases in the presence of serine (Fig. 4*B*). Although Tsr^{gg} [QQQQE] exhibited locked-ON output in FRET kinase assays (*SI Appendix*, Table S3), it did show a robust crosslinking response to serine, indicating that serine-induced conformational changes at the MH cap are more sensitive than are the serine kinase control responses in Tsr core signaling complexes.

Signaling Properties of Tsr^{gg} Receptors with and without BMOE-Induced Crosslinks. We examined all single- and double-cysteine receptors, the G268P and D269P, and the

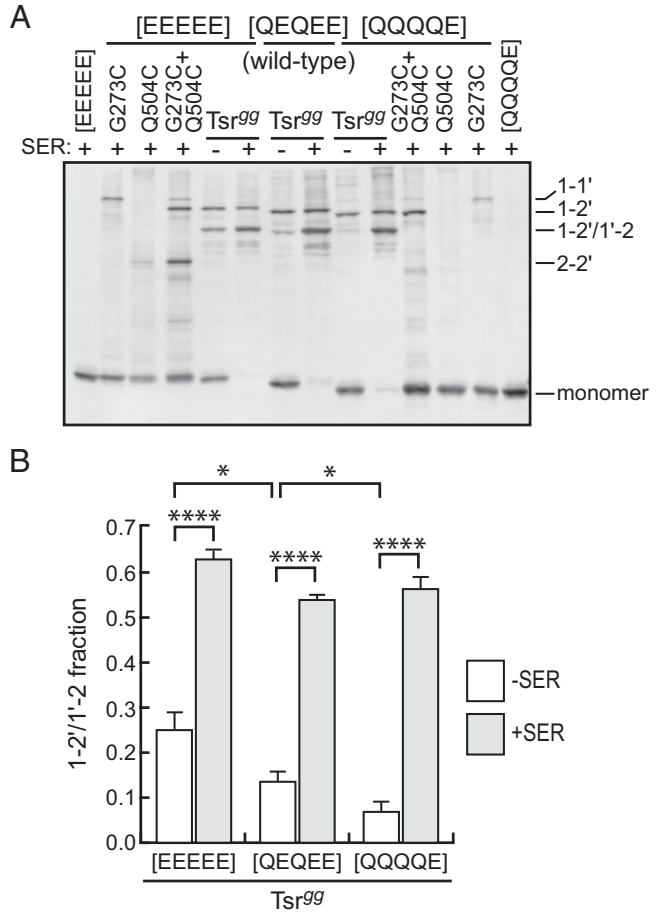

Fig. 4. Crosslinking of Tsr^{gg} receptors in different modification states. (*A*) SDS-PAGE immunoblot of BMOE crosslinking products. Tsr^{gg} receptors in [EEEEE], [QEQEE] (wild-type), or [QQQQE] modification states were expressed in strain UU2610 in the presence and absence of serine and treated with BMOE for 1.5 min. (*B*) Quantification of crosslinking results from three independent replicates of the experiment in *A*. Histogram bars show the mean ± SD fraction of doubly crosslinked Tsr subunits in the samples. Asterisks denote a significant difference based on a *P* value of <0.0001 (****) or <0.05 (*).

[EEEEE] and [QQQQE] derivatives of Tsr^{gg} with FRET kinase assays to compare their signaling properties to those of wild-type Tsr (*SI Appendix*, Table S3). The host strain for the FRET experiments was UU2567, a close relative of the *Δmcp ΔcheRB* UU2610 strain used in the crosslinking experiments. As in the crosslinking experiments, UU2567 lacks the CheR and CheB enzymes, thereby ensuring a homogeneous population of receptor molecules. Most single-cysteine receptors had ON-shifted behaviors, but the G273C and Q504C serine response thresholds were only about fourfold and eightfold higher than the wild type. Tsr^{gg} with both of those cysteine sites had a serine response threshold ~20-fold above that of the wild type but nevertheless mediated wild-type chemotaxis in an adaptation-competent host (*SI Appendix*, Fig. S1 *B* and *C*). ON- and OFF-shifting alterations had additive effects on the detection sensitivity of Tsr^{gg}. For example, the OFF-shifting [EEEEE] modification reduced the serine response threshold of Tsr^{gg} more than 25-fold; the more strongly OFF-shifting D269P lesion lowered the Tsr^{gg} response threshold about 200-fold (D269P). The moderately ON-biased [QQQQE] modification shifted Tsr^{gg} to locked-ON kinase output (*SI Appendix*, Table S3).

The 1-2'/1'-2 crosslinked species of Tsr^{gg} appears to represent a kinase-OFF output conformation of the MH cap because it accumulated in the presence of serine and in combination with the locked-OFF D269P and [EEEEE] variants. As a critical test of this idea, we assessed the signaling properties of Tsr^{gg} reporters with FRET kinase experiments before and after subjecting the same cells to BMOE-induced crosslinking. We first asked whether BMOE treatment would perturb the serine dose response behavior of wild-type Tsr, which has no native cysteines. The $K_{1/2}$ for wild-type Tsr, or serine concentration that reduces activity to 50%, was evaluated in host strain UU2567 and found to be 18 μM (*SI Appendix*, Fig. S8*A*). A subsequent 100 s BMOE pulse caused a modest decrease in YFP/CFP ratio, but the cells remained responsive to serine with unchanged sensitivity ($K_{1/2}$ = 18 μM). A second BMOE pulse in combination with a saturating serine stimulus had essentially no effect on the kinase activity or serine responsiveness of the cells ($K_{1/2}$ = 16 μM) (*SI Appendix*, Fig. S8*A*). The partial decline in kinase activity following the initial BMOE pulse could be due to modification of some other component of the signaling system. Although CheW, CheY, and CheZ contain no native cysteines, CheA contains three (C120, C215, C410), which are not critical to its signaling functions (43, 44). In UU3045, a host encoding a cysteine-free CheA (C120S/C225S/C410S), wild-type Tsr showed signaling behaviors comparable to those in the wild-type CheA host (*SI Appendix*, Fig. S8*B*). After the first BMOE pulse, there was still some drop in FRET signal, which might be caused by BMOE modification of the YFP and/or CFP FRET reporters, both of which contain two cysteine residues. We conclude from these wild-type Tsr tests that BMOE exposure did not substantially impair the function of wild-type CheA, so we used a native CheA host for subsequent FRET experiments with Tsr^{gg} receptors.

Unlike wild-type Tsr, Tsr^{gg} showed substantial signaling changes upon BMOE exposure (Fig. 5*A*). An initial 100 s BMOE pulse improved the serine sensitivity of Tsr^{gg} from a $K_{1/2}$ of 410 μM to 150 μM, consistent with a shift toward the kinase-OFF state. Recall that in the absence of serine, BMOE treatment crosslinked only ~20% of Tsr^{gg} in the 1-2'/1'-2 form (Fig. 2 and *SI Appendix*, Fig. S3 *E* and *F*). A saturating serine stimulus in combination with BMOE treatment, conditions that crosslinked ~60% of Tsr^{gg} in the 1-2'/1'-2 form (Fig. 2 and *SI Appendix*, Fig. S3 *E* and *F*), locked Tsr^{gg} output in the kinase-OFF state (Fig. 5*A*). In combination with the strongly ON-shifting G268P lesion, Tsr^{gg} failed to respond to serine and maintained high kinase activity, detectable by KCN treatment, both before and after BMOE pulses (Fig. 5*B*). Although the ON-shifting properties of Tsr^{gg} rendered the OFF-shifting D269P lesion serine responsive, BMOE treatment alone locked it in the kinase-OFF state (Fig. 5*B*). In summary, these results strongly support our contention that the BMOE-crosslinked form of Tsr^{gg} represents the kinase-OFF structural state of the MH cap.

This conclusion holds, as well, for three other adjacent *g-g* cysteine pairs in the MH cap. The G273C/A511C, G280C/Q504C, and G287C/A497C Tsr reporters all showed BMOE-induced shifts toward the kinase-OFF output state (Fig. 6). Tsr-G280C/A497C, which could not support chemotaxis in soft agar assays (*SI Appendix*, Fig. S1*A*), exhibited locked-ON output behavior both before and after BMOE exposure. This combination of cysteine replacements evidently prevents the Tsr MH cap from reaching the kinase-OFF conformation. This receptor also produced fewer 1-2'/1'-2 products than did the other adjacent reporter pairs (*SI Appendix*, Fig. S1*B*). In combination with Q504C, G280C locked output in a nonresponsive ON state, but Tsr-G280C/Q504C did become partially

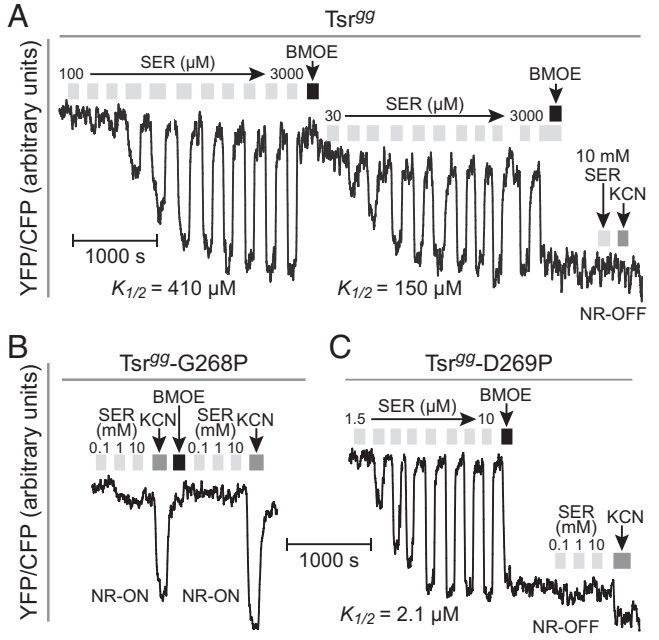

Fig. 5. Signaling behaviors of Tsr^{gg} receptors before and after BMOE crosslinking. CheA activities were measured with in vivo FRET kinase assays. All plots are shown at the same scale. Light-gray boxes mark serine exposures at the indicated concentrations; black boxes mark exposures to 200 μM BMOE; dark-gray boxes mark exposures to 3 mM KCN. Stacked boxes in *A* and *B* indicate an initial serine exposure, followed by BMOE with serine remaining present. Values for the response $K_{1/2}$ are listed for each serine dose response series. NR-ON, nonresponsive kinase activity; NR-OFF, no kinase activity or response. (*A*) Tsr^{gg} responses. (*B*) Tsr^{gg}-G268P responses. (*C*) Tsr^{gg}-D269P responses.

responsive to serine after BMOE exposure (Fig. 6 and *SI Appendix*, Fig. S8*C*). Together, these findings indicate that Tsr output shifts toward the kinase-OFF state upon BMOE crosslinking of cysteines at adjacent MH1-MH2' *g* sites in the MH cap (see Fig. 1*B*). Thus, the ability to serve as an output state reporter is not unique to the Tsr^{gg} receptor but rather a general feature of adjacent *g-g* cysteine pairs in the MH cap region.

Discussion

This study describes in vivo crosslinking readouts for signaling-related structural changes in the cytoplasmic domain of the *E. coli* serine chemoreceptor Tsr. The crosslinking reporter sites themselves had only modest effects on Tsr signaling properties, enabling us to evaluate receptor output states before and after crosslink formation. Below, we discuss these results in the context of a working model for Tsr signal transmission and suggest that similar crosslinking approaches could serve to follow signal transmission in other regions of the chemoreceptor molecule and perhaps in other signaling proteins, as well.

A Model for Signal Propagation between the Tsr HAMP and MH Cap Four-Helix Bundles. Although there are no high-resolution, experimentally determined structures available for the Tsr HAMP domain, its primary structure (13), as well as mutational and functional studies (25, 40, 45), suggests close similarity to the principal structural features of the Af1503 HAMP domain. That HAMP domain comprises a parallel, four-helix bundle capable of two distinct packing modes, a canonical knobs-into-holes *a-d* arrangement and a less conventional complementary *x-da* arrangement (Fig. 7). In both the Af1503 and Tsr HAMP domains, the *a-d* mode corresponds to an OFF-output conformation; the *x-da* mode represents an ON-output state (40, 46). Transitions between these two alternative structures likely proceed through unstable intermediate conformations. Single amino acid replacements at key packing residues probably perturb HAMP signal output by stabilizing such intermediates (46).

Experimental (47, 48) and computational (23) studies of Tsr and other MCPs indicate that their antiparallel four-helix methylation bundles also adopt *a-d* and *x-da* packing arrangements (Fig. 7). In Tsr (and other HAMP-containing MCPs and sensory kinases), the HAMP AS2 output helices connect to the MH1 helices through a four-residue "phase stutter" (13). The stutter imposes conflicting packing registers on the AS2 and MH1 helices, as follows: strong *a-d* packing in HAMP probably shifts the MH cap to an *x-da* packing arrangement, whereas *x-da* HAMP packing probably favors an *a-d* packing arrangement of the cap.

These structural considerations imply that the MH cap transitions from the kinase-ON to the kinase-OFF state through an AS2-imposed torque on MH1, in a clockwise direction if viewed inward from the membrane (Fig. 7). The resultant MH1 rotation should shift *d* packing residues toward the hydrophobic core of the bundle and *g* residues into a flanking (*x-da*) position, as seen in the crystal structure of a chimeric protein containing Af1503-HAMP joined to the MH cap through the hairpin tip portion of Tsr (48). For simplicity, we propose that the kinase-ON and kinase-OFF MH cap output states correspond to discrete coiled-coil packing conformations (*a-d* and *x-da*, respectively). However, transitions between these conformations probably occur through a range of intermediate states analogous to those seen in mutant Af1503 HAMP constructs (46). Much of the experimental in vitro work on MH cap structure, primarily in the closely related Tar (aspartate) receptor, indicates that the MH1 helices have dynamic behaviors that reflect fluctuations in helicity and helix-packing strength. These bundle breathing motions are generally less pronounced in the MH2 helices (15–18, 20–22). Moreover, the OFF state cap may enhance MH2 structural interactions (17), whereas MH1 structural interactions become less favorable (17, 18). Accordingly, we envision several possible MH cap transition states with the predominant one featuring MH2/MH2' coiled-coils (Fig. 7) (49).

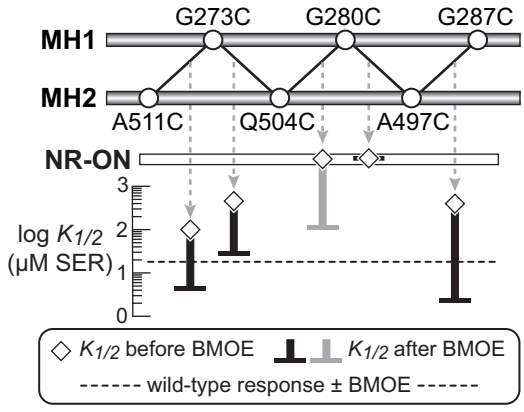

Fig. 6. Signaling properties of Tsr MH cap *g-g* cysteine reporters before and after BMOE crosslinking. MH1 *g* heptad position cysteines (G273C, G280C, G287C) were combined pairwise with flanking (adjacent in the native cap) MH2 *g* heptad position cysteines (A511C, Q504C, A497C) and tested for serine responses and kinase activity with in vivo FRET assays. Black lines connecting cysteine replacements indicate the pairwise combinations tested in UU2567 cells. The G280C/Q504C receptor only controlled a fraction of available kinase activity after BMOE treatment (gray symbol; *SI Appendix*, Fig. S7*C*). NR-ON, nonresponsive to serine and kinase-ON.

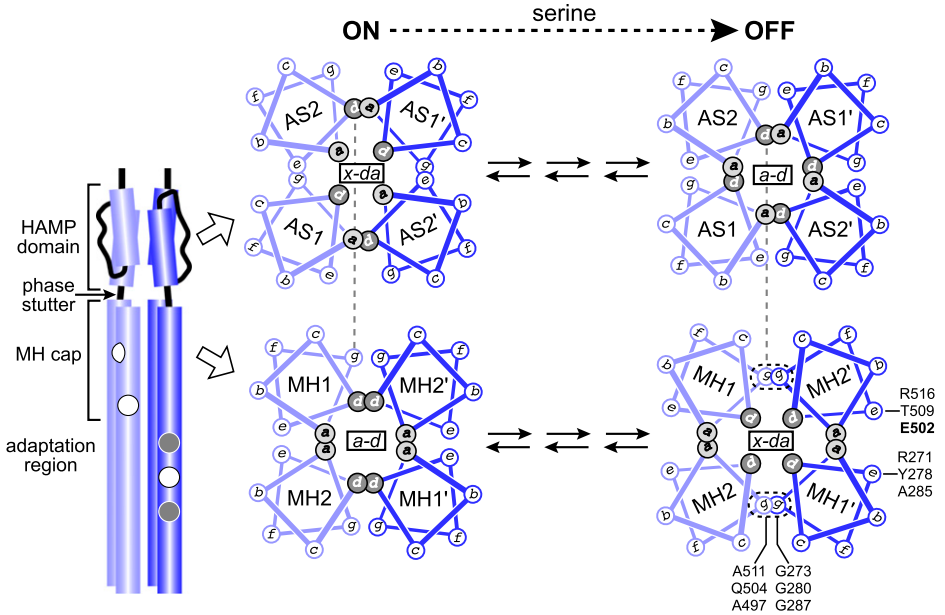

Fig. 7. A model of output state structural features in the Tsr HAMP and MH cap signaling elements. Helical wheels depict cross-sections of helix-packing arrangements in the OFF and ON output states. The four-helix HAMP bundle may shift between two discrete limit conformations (*a-d* and *x-da* packing) (61) via a number of dynamic intermediates (forward/reverse arrow pairs) (12, 40, 62). The OFF-state HAMP bundle is pictured in a canonical *a-d* packing arrangement (40, 46, 61). The ON state is shown in an *x-da* arrangement (12, 40, 61, 62) in which the *g* (AS1) and *e* (AS2) edge residues rotate into and contribute to the packing interface. The four-residue phase stutter joining HAMP to the MH cap (shown for one subunit as a dashed line) puts the packing faces of the AS2 and MH1 helices out of register, imposing different optimal packing arrangements on the HAMP and MH cap bundles. For example, the third stutter residue has a *d* position in the AS2 phase, but a *g* position in the MH1 phase. Serine stimuli that drive HAMP to the OFF state should, therefore, favor an *x-da* packing arrangement in the MH cap, in which opposed *g* residues move closer to one another, a structural change that is consistent with our crosslinking results. The alternative MH cap ON state might pack as an *a-d* bundle. Structural intermediates between the MH cap ON and OFF states should arise through transient melting of the helix-helix interactions and partner shuffles. MH1 helices are less stable and pack with one another less frequently than do MH2 helices (20, 21).

Evidence for Different MH Cap Helix-Packing Modes in Different Output States. Our crosslinking studies indicated that the MH cap OFF-output state, elicited by an attractant stimulus or by an OFF-shifting structural change (D269P) or adaptational modification [EEEEE], brought *g*-position cysteine reporters in the MH1 and MH2 helices into close proximity. Conversely, an MH cap in the ON state, either in the absence of an attractant stimulus or elicited by an ON-shifting structural change (G268P) or adaptational modification [QQQQE], reduced *g*-position crosslinking threefold or more. These results are consistent with clockwise rotation of MH1 cap *g*-position residues into the bundle-packing interface in the OFF-output state (Fig. 7). To reach the stable OFF conformation, the bundle would need to breathe, thereby enabling the MH2 helices to shift in a counterclockwise direction to form the proposed *x-da* packing arrangement (Fig. 7). The crosslinking behaviors of single-cysteine replacements in the MH cap probably reflect dynamic helix motions; we observed both MH1-MH1' and MH2-MH2' crosslinked species (*SI Appendix*, Fig. S1*B*), consistent with bundle breathing movements that occasionally allow close, unhindered interactions between cognate helices.

The primary structures of Tsr and related receptors offer additional, albeit circumstantial, evidence for this helix breathing-axial rotation-bundle repacking signaling mechanism. In Tsr, for example, the *g*-position cap residues have small sidechains, either glycine (at 3/3 MH1 positions) or alanine (at 2/3 MH2 positions) (Figs. 1*D* and 7). By contrast, the HAMP-proximal *e*-position cap residues have large sidechains, as follows: arginine and tyrosine at the first two MH1 positions and arginine at the first MH2 position (Figs. 1*D* and 7). These sidechain differences would be expected to favor closer apposition of the *g* positions than the *e* positions, conceivably poising the MH cap for attractant-induced transition to the OFF-output state. According to this scenario, crosslinks between cysteine replacements at *e* positions should shift receptor output toward the kinase-ON state; we are currently testing that prediction.

Crosslinking Effects of Conformational Input from the Adaptation Sites. In addition to helix-torquing inputs from HAMP, the MH cap receives conformational influence from the adjoining methylation-site helices, which may also transition between *a-d* and *x-da* packing modes (48). Given that there are no phase stutters or other register shifts between the MH cap and adaptation segments of the receptor, these regions might have helix-packing arrangements in common. Accordingly, modification states that favor *x-da* packing of the methylation helices could favor *x-da* packing of the MH cap, which is the conformation our model assigns to the OFF-output state. It then follows that the [EEEEE] modification state, which promoted OFF-state crosslinking behavior of the cap, should adopt an *x-da* packing mode in the adaptation region. However, circumstantial evidence suggests that this may not be the case. The four orthodox methylation sites in MH1 and MH2 lie at solvent-exposed *c* heptad positions, flanked by adjacent glutamate residues at *b* positions and additional acidic residues at *c* positions in neighboring heptads (10, 50). In the [EEEEE] modification state, MH1 has eight acidic residues along the solvent-exposed face of four contiguous heptads; MH2 has six acidic residues at *b* or *c* positions in the corresponding four-heptad segment. Mutational analyses of these acidic residues in Tar indicated that a high density of negative charges along the outward faces of the adaptation helices might affect output state by reducing the stability of those helices (50). Reduced helix stability should

enhance bundle-breathing episodes, leading to dynamic behaviors of the MH1 helices in the [EEEEE] modification state (15, 16, 18). According to this structural scenario, the [EEEEE] receptor produces OFF-shifted output, not because it promotes *x-da* packing but because it destabilizes the *a-d* packing arrangement associated with the ON output state, thereby allowing conformational input from HAMP to dominate the MH cap packing arrangement. Thus, attractant stimuli elicit OFF output by stabilizing *x-da* packing of the cap, whereas the [EEEEE] receptor might produce OFF output by destabilizing the *a-d* packing arrangement of the cap. Although the [EEEEE] structural state has long served as a proxy for the attractant-induced OFF conformation, that structural equivalency may be unjustified.

The disparate serine sensitivities of the Tsr^{gg} [QQQQE] receptor in cap crosslinking and FRET kinase assays provide additional context for this idea. Tsr^{gg} [QEQEE] responded to serine, whereas Tsr^{gg} [QQQQE] had locked-ON kinase output in FRET experiments. However, their BMOE crosslinking responses to serine stimuli were comparable; both receptors produced substantial OFF-output patterns. These findings suggest that structural changes induced by ligand occupancy may be different from those produced by modification state changes. Moreover, EPR studies that detected structural differences between Tar [EEEE] and Tar [QQQQ] receptors in nanodiscs, consistent with their different output states, did not detect any change of Tar [QQQQ] structure in response to an aspartate stimulus (21). Together, these observations indicate caution is advisable when attempting to mimic the ligand-induced signaling state of a receptor by manipulating a different structural parameter.

The *g-g* Crosslinking Signal Provides a Structural Snapshot of Receptor Output Conformation and/or Dynamics. If we assume that only the OFF-state cap can produce a fully crosslinked (1-2'/1'-2) Tsr dimer, then the low crosslinking signals of receptors with ON-shifted output would imply that they were capable of occasional transitions to the OFF conformation. However, longer crosslinking reactions did not lead to an ever-increasing fraction of crosslinking products from any of the tested receptors. Regardless of their output state, the BMOE crosslinking reactions reached a maximum extent in less than 2 min. This behavior implies exhaustion of the reaction chemistry, perhaps through a reaction of BMOE with glutathione and other thiol-containing cell components. Thus, our end-point crosslinking signals essentially reflect the equilibrium proportions of ON and OFF states and their rates of interconversion over the course of a 2-min reaction. For simplicity, we have assumed that these alternative output states are discrete conformations with different reporter site geometries. However, state-dependent changes in the frequency or amplitude of dynamic structural motions can also influence crosslinking propensity by modulating the rate of productive encounters between reporter sites. It might be possible to assess the relative contributions of structural and dynamic factors to Tsr^{gg} crosslinking signals with more extensive studies of single-cysteine receptors, which presumably form crosslinks through dynamic motions of the receptor subunits.

Experimental Extensions of Our In Vivo Crosslinking Approach. In vivo studies of receptor molecules fluorescently tagged at their C termini have demonstrated trimer-dependent conformational responses to attractant stimuli; OFF-shifts increase the distance between trimer members, and ON-shifts reduce interdimer distances (51). BMOE-induced crosslinking at *g-g* heptad positions in the Tsr MH cap produced similar results in both core complexes and receptor trimers, but it seems likely that the assay reports on the stimulus-induced conformational changes of individual receptor dimers, comparable to those observed in solitary dimers in nanodiscs (32). These dimer-level conformational changes presumably underlie the movements of receptors in trimers-of-dimers and in core signaling complexes. At the cap, crosslinking at *g-g* heptad positions shifted receptor output toward the kinase-OFF state, consistent with transition to an *x-da* helix-packing mode. If the ON-state cap has an *a-d* packing arrangement, we should find that crosslinking at *e-e* heptad positions shifts receptor output toward the ON state. If so, then these in vivo crosslinking tools could serve to probe helix-packing transitions and their output consequences in other segments of the extended receptor cytoplasmic domain. Moreover, similar crosslinking approaches could prove valuable in exploring stimulus-induced conformational changes in other signaling proteins.

Materials and Methods

Bacterial Strains and Growth Conditions. All *E. coli* strains used in this study are derivatives of RP437 (52) with deletions of all chromosomal MCP genes (*SI Appendix*, Table S2). Unless otherwise noted, bacteria were grown in tryptone broth (1% tryptone and 0.5% NaCl wt/vol) at 30 °C with shaking. Standard antibiotic concentrations for plasmid maintenance were 100 μg/mL for ampicillin and 25 μg/mL for chloramphenicol.

Plasmids. Plasmid pRR53 confers ampicillin resistance and carries the *tsr* coding region under IPTG-inducible *tac* promoter control (24). Compatible plasmid pPA114 confers chloramphenicol resistance and expresses *tsr* under inducible sodium salicylate control. Site-directed *tsr* mutations were constructed in pRR53 and pPA114 by QuikChange PCR mutagenesis and verified by sequencing the entire protein-coding region (24). FRET reporter plasmid pRZ30 expresses *cheY-yfp* and *cheZ-cfp* gene fusions under salicylate control (40).

Quantifying the Expression of Mutant Tsr Proteins. Assays were performed as previously described (53). Briefly, overnight cultures of strain UU2610 carrying *tsr* expression plasmids were diluted 1:100 into tryptone broth containing appropriate inducer and antibiotic concentrations (pRR53: 100 μM IPTG and 50 μg/mL ampicillin; pPA114: 0.6 μM sodium salicylate and 12.5 μg/mL chloramphenicol). Cells were grown to midexponential phase, washed, then resuspended in 2× Laemmli sample buffer (54) containing 5% β-mercaptoethanol, and boiled for 5 min. Whole-cell lysates were analyzed by denaturing gel electrophoresis (SDS-PAGE; 11% polyacrylamide). Gels were immunoblotted with polyclonal rabbit antiserum directed against the highly conserved Tsr signaling domain (55) and a Cy5-labeled goat anti-rabbit antibody (ThermoFisher, catalog no. A10523). Western blots were imaged under fluorescence mode in a Typhoon FLA 9500 scanner (GE Healthcare), and bands were quantified with ImageJ (56).

Chemotaxis Assays. The receptor-less host strain UU2612 was transformed with *tsr* expression plasmid pRR53 or derivatives, and individual transformant colonies were inoculated to tryptone plates containing 0.25% agar, 100 μM IPTG, and 50 μg/mL ampicillin. Plates were incubated at 32.5 °C for 6 to 8 h.

BMOE Crosslinking Assays. Strains UU2610 (*cheA*$^{+}$*W*$^{+}$) or UU2806 (Δ*cheAW*) were transformed with mutant derivatives of pRR53, pPA114, or both. Overnight cultures of transformed strains were grown at 30 °C in tryptone broth with appropriate antibiotics and then diluted 1:100 into tryptone broth containing appropriate inducer and antibiotic concentrations (pRR53: 100 μM IPTG and 50 μg/mL ampicillin; pPA114: 0.6 μM sodium salicylate and 12.5 μg/mL chloramphenicol; pRR53+pPA114: 50 μM IPTG, 0.3 μM sodium salicylate, 50 μg/mL ampicillin and 12.5 μg/mL chloramphenicol). Cells were grown at 30 °C to midexponential phase (optical density at 600 nm = 0.5), and 1-mL aliquots were harvested (16,000 × *g*, 3 min), washed with 1 mL tethering buffer (57), and then resuspended in 1 mL tethering buffer containing different

concentrations of serine. Cells were incubated in the presence of serine for 20 min at 30 °C. Crosslinking was accomplished by treating cells with 200 μM BMOE (Thermo Scientific) in dimethyl sulfoxide (DMSO) at 30 °C, with DMSO alone serving as the negative control. Samples at each time point were treated with N-ethylmaleimide at a final concentration of 10 mM to quench the BMOE reaction. Cells were pelleted (21,000 × *g*, 2 min), lysed by resuspension in 50 μl 2× Laemmli sample buffer (54), and boiled for 5 min. Reduced samples were combined in a 1:1 ratio with 2× Laemmli buffer containing 350 mM DTT and boiled for 10 min. Whole-cell lysates were analyzed by SDS-PAGE using 9% gels and transferred to polyvinylidene fluoride membranes. Immunoblotting and data analysis were performed as described above.

Disulfide Crosslinking Assays. Strain UU2610 ($cheA^+W^+$) was transformed with mutant derivatives of pRR53, pPA114, or both. Cell growth conditions, antibiotic and inducer concentrations, volumes harvested, centrifuge speeds, and reducing conditions are described in the previous section. Cells were washed with phosphate-buffered saline and incubated at 30 °C for 20 min and then were treated with 300 μM Cu^{2+}-phenanthroline at 30 °C for 10 min to induce disulfide formation. The reaction was quenched with 10 mM sodium EDTA (pH 8). Cell lysates were prepared and processed as described above.

Statistics. Statistical calculations were performed in Microsoft Excel (version 15.33 for Mac) using Student's *t* test.

Adaptational Modification Assays. Tsr modification tests were performed as previously described (57). Briefly, derivatives of *tsr* expression plasmid pRR53 were transformed into host strains UU2632 (R^+B^-), UU2611 (R^-B^+), and UU2612 (R^+B^+). Cells were grown to midexponential phase at 30 °C in tryptone broth containing 100 μM IPTG and 50 μg/mL ampicillin, washed in tethering buffer, and then exposed to 10 mM serine for 20 min. Cells were washed again, lysed by boiling in 2× Laemmli buffer, and analyzed by low-bis SDS-PAGE (58). Tsr protomers were visualized and quantified as described above.

In Vivo FRET-Based Kinase Assays. The experimental setup, assays, and data analyses have been described (36, 39, 40). Strains UU2567 or UU3045 (*SI Appendix*, Table S2) were transformed with pRZ30 and pRR53 derivatives. BMOE was at 200 μM for 100 s followed by at least a 100 s wash with tethering buffer before further test solutions. Cells that failed to respond to 10 mM serine were tested with 3 mM KCN to determine CheA activity state (40).

Protein Structure Models. PyMOL (Schrödinger software) was used to visualize and create amino acid replacements in atomic structures.

Data Availability. All study data are included in the article and/or *SI Appendix*.

ACKNOWLEDGMENTS. Thanks to Peter Ames (University of Utah) and Lynmarie Thompson (University of Massachusetts) for discerning comments on a draft version of the manuscript. This work was supported by Research Grant GM19559 (J.S.P.) from the National Institute of General Medical Sciences. The Protein-DNA Core Facility at the University of Utah receives support from National Cancer Institute Grant CA42014 to the Huntsman Cancer Institute.

1. B. E. Scharf, M. F. Hynes, G. M. Alexandre, Chemotaxis signaling systems in model beneficial plant-bacteria associations. *Plant Mol. Biol.* **90**, 549–559 (2016).
2. M. Erhardt, Strategies to block bacterial pathogenesis by interference with motility and chemotaxis. *Curr. Top. Microbiol. Immunol.* **398**, 185–205 (2016).
3. M. A. Matilla, T. Krell, The effect of bacterial chemotaxis on host infection and pathogenicity. *FEMS Microbiol. Rev.* **42**, fux052 (2018).
4. R. Colin, B. Ni, L. Laganenka, V. Sourjik, Multiple functions of flagellar motility and chemotaxis in bacterial physiology. *FEMS Microbiol. Rev.* **45**, fuab038 (2021).
5. G. L. Hazelbauer, J. J. Falke, J. S. Parkinson, Bacterial chemoreceptors: High-performance signaling in networked arrays. *Trends Biochem. Sci.* **33**, 9–19 (2008).
6. J. S. Parkinson, G. L. Hazelbauer, J. J. Falke, Signaling and sensory adaptation in *Escherichia coli* chemoreceptors: 2015 update. *Trends Microbiol.* **23**, 257–266 (2015).
7. S. Bi, V. Sourjik, Stimulus sensing and signal processing in bacterial chemotaxis. *Curr. Opin. Microbiol.* **45**, 22–29 (2018).
8. M. Li, G. L. Hazelbauer, Core unit of chemotaxis signaling complexes. *Proc. Natl. Acad. Sci. U.S.A.* **108**, 9390–9395 (2011).
9. G. E. Piñas, V. Frank, A. Vaknin, J. S. Parkinson, The source of high signal cooperativity in bacterial chemosensory arrays. *Proc. Natl. Acad. Sci. U.S.A.* **113**, 3335–3340 (2016).
10. R. P. Alexander, I. B. Zhulin, Evolutionary genomics reveals conserved structural determinants of signaling and adaptation in microbial chemoreceptors. *Proc. Natl. Acad. Sci. U.S.A.* **104**, 2885–2890 (2007).
11. K. E. Swain, M. A. Gonzalez, J. J. Falke, Engineered socket study of signaling through a four-helix bundle: Evidence for a yin-yang mechanism in the kinase control module of the aspartate receptor. *Biochemistry* **48**, 9266–9277 (2009).
12. Q. Zhou, P. Ames, J. S. Parkinson, Mutational analyses of HAMP helices suggest a dynamic bundle model of input-output signalling in chemoreceptors. *Mol. Microbiol.* **73**, 801–814 (2009).
13. J. S. Parkinson, Signaling mechanisms of HAMP domains in chemoreceptors and sensor kinases. *Annu. Rev. Microbiol.* **64**, 101–122 (2010).
14. S. S. Koshy, S. J. Eyles, R. M. Weis, L. K. Thompson, Hydrogen exchange mass spectrometry of functional membrane-bound chemotaxis receptor complexes. *Biochemistry* **52**, 8833–8842 (2013).
15. S. S. Koshy, X. Li, S. J. Eyles, R. M. Weis, L. K. Thompson, Hydrogen exchange differences between chemoreceptor signaling complexes localize to functionally important subdomains. *Biochemistry* **53**, 7755–7764 (2014).
16. X. Li, S. J. Eyles, L. K. Thompson, Hydrogen exchange of chemoreceptors in functional complexes suggests protein stabilization mediates long-range allosteric coupling. *J. Biol. Chem.* **294**, 16062–16079 (2019).
17. M. Kashefi, L. K. Thompson, Signaling-related mobility changes in bacterial chemotaxis receptors revealed by solid-state NMR. *J. Phys. Chem. B* **121**, 8693–8705 (2017).
18. N. Malik, K. A. Wahlbeck, L. K. Thompson, Strategies for identifying dynamic regions in protein complexes: Flexibility changes accompany methylation in chemotaxis receptor signaling states. *Biochim. Biophys. Acta Biomembr.* **1862**, 183312 (2020).
19. D. Samanta, P. P. Borbat, B. Dzikovski, J. H. Freed, B. R. Crane, Bacterial chemoreceptor dynamics correlate with activity state and are coupled over long distances. *Proc. Natl. Acad. Sci. U.S.A.* **112**, 2455–2460 (2015).
20. N. L. Bartelli, G. L. Hazelbauer, Differential backbone dynamics of companion helices in the extended helical coiled-coil domain of a bacterial chemoreceptor. *Protein Sci.* **24**, 1764–1776 (2015).
21. N. L. Bartelli, G. L. Hazelbauer, Bacterial chemoreceptor dynamics: Helical stability in the cytoplasmic domain varies with functional segment and adaptational modification. *J. Mol. Biol.* **428**, 3789–3804 (2016).
22. J. B. Gordon *et al.*, Concerted differential changes of helical dynamics and packing upon ligand occupancy in a bacterial chemoreceptor. *ACS Chem. Biol.* **16**, 2472–2480 (2021).
23. D. R. Ortega *et al.*, A phenylalanine rotameric switch for signal-state control in bacterial chemoreceptors. *Nat. Commun.* **4**, 2881 (2013).
24. P. Ames, C. A. Studdert, R. H. Reiser, J. S. Parkinson, Collaborative signaling by mixed chemoreceptor teams in *Escherichia coli*. *Proc. Natl. Acad. Sci. U.S.A.* **99**, 7060–7065 (2002).
25. P. Ames, Q. Zhou, J. S. Parkinson, Mutational analysis of the connector segment in the HAMP domain of Tsr, the *Escherichia coli* serine chemoreceptor. *J. Bacteriol.* **190**, 6676–6685 (2008).
26. S. Kitanovic, P. Ames, J. S. Parkinson, A trigger residue for transmembrane signaling in the *Escherichia coli* serine chemoreceptor. *J. Bacteriol.* **197**, 2568–2579 (2015).
27. K. K. Kim, H. Yokota, S. H. Kim, Four-helical-bundle structure of the cytoplasmic domain of a serine chemotaxis receptor. *Nature* **400**, 787–792 (1999).
28. C. A. Studdert, J. S. Parkinson, Crosslinking snapshots of bacterial chemoreceptor squads. *Proc. Natl. Acad. Sci. U.S.A.* **101**, 2117–2122 (2004).
29. R. B. Bass, M. D. Coleman, J. J. Falke, Signaling domain of the aspartate receptor is a helical hairpin with a localized kinase docking surface: Cysteine and disulfide scanning studies. *Biochemistry* **38**, 9317–9327 (1999).
30. G. Li, R. M. Weis, Covalent modification regulates ligand binding to receptor complexes in the chemosensory system of *Escherichia coli*. *Cell* **100**, 357–365 (2000).
31. D. N. Amin, G. L. Hazelbauer, Chemoreceptors in signalling complexes: Shifted conformation and asymmetric coupling. *Mol. Microbiol.* **78**, 1313–1323 (2010).
32. D. N. Amin, G. L. Hazelbauer, The chemoreceptor dimer is the unit of conformational coupling and transmembrane signaling. *J. Bacteriol.* **192**, 1193–1200 (2010).
33. D. L. Milligan, D. E. Koshland, Jr., Purification and characterization of the periplasmic domain of the aspartate chemoreceptor. *J. Biol. Chem.* **268**, 19991–19997 (1993).
34. K. E. Swain, J. J. Falke, Structure of the conserved HAMP domain in an intact, membrane-bound chemoreceptor: A disulfide mapping study. *Biochemistry* **46**, 13684–13695 (2007).
35. H. Tajima *et al.*, Ligand specificity determined by differentially arranged common ligand-binding residues in bacterial amino acid chemoreceptors Tsr and Tar. *J. Biol. Chem.* **286**, 42200–42210 (2011).
36. V. Sourjik, H. C. Berg, Receptor sensitivity in bacterial chemotaxis. *Proc. Natl. Acad. Sci. U.S.A.* **99**, 123–127 (2002).
37. P. Dunten, D. E. Koshland, Jr., Tuning the responsiveness of a sensory receptor via covalent modification. *J. Biol. Chem.* **266**, 1491–1496 (1991).
38. G. L. Hazelbauer, W. C. Lai, Bacterial chemoreceptors: Providing enhanced features to two-component signaling. *Curr. Opin. Microbiol.* **13**, 124–132 (2010).
39. V. Sourjik, A. Vaknin, T. S. Shimizu, H. C. Berg, In vivo measurement by FRET of pathway activity in bacterial chemotaxis. *Methods Enzymol.* **423**, 365–391 (2007).
40. R. Z. Lai, J. S. Parkinson, Functional suppression of HAMP domain signaling defects in the *E. coli* serine chemoreceptor. *J. Mol. Biol.* **426**, 3642–3655 (2014).
41. M. S. Rice, F. W. Dahlquist, Sites of deamidation and methylation in Tsr, a bacterial chemotaxis sensory transducer. *J. Biol. Chem.* **266**, 9746–9753 (1991).
42. X. S. Han, J. S. Parkinson, An unorthodox sensory adaptation site in the *Escherichia coli* serine chemoreceptor. *J. Bacteriol.* **196**, 641–649 (2014).
43. A. S. Miller, S. C. Kohout, K. A. Gilman, J. J. Falke, CheA Kinase of bacterial chemotaxis: Chemical mapping of four essential docking sites. *Biochemistry* **45**, 8699–8711 (2006).
44. J. Zhao, J. S. Parkinson, Cysteine-scanning analysis of the chemoreceptor-coupling domain of the *Escherichia coli* chemotaxis signaling kinase CheA. *J. Bacteriol.* **188**, 4321–4330 (2006).
45. P. Ames, Q. Zhou, J. S. Parkinson, HAMP domain structural determinants for signalling and sensory adaptation in Tsr, the *Escherichia coli* serine chemoreceptor. *Mol. Microbiol.* **91**, 875–886 (2014).
46. H. U. Ferris *et al.*, The mechanisms of HAMP-mediated signaling in transmembrane receptors. *Structure* **19**, 378–385 (2011).
47. A. M. Pollard, A. M. Bilwes, B. R. Crane, The structure of a soluble chemoreceptor suggests a mechanism for propagating conformational signals. *Biochemistry* **48**, 1936–1944 (2009).

48. H. U. Ferris, K. Zeth, M. Hulko, S. Dunin-Horkawicz, A. N. Lupas, Axial helix rotation as a mechanism for signal regulation inferred from the crystallographic analysis of the *E. coli* serine chemoreceptor. *J. Struct. Biol.* **186**, 349–356 (2014).
49. C. E. Flack, J. S. Parkinson, A zipped-helix cap potentiates HAMP domain control of chemoreceptor signaling. *Proc. Natl. Acad. Sci. U.S.A.* **115**, E3519–E3528 (2018).
50. D. J. Starrett, J. J. Falke, Adaptation mechanism of the aspartate receptor: Electrostatics of the adaptation subdomain play a key role in modulating kinase activity. *Biochemistry* **44**, 1550–1560 (2005).
51. V. Frank, A. Vaknin, Fluorescence anisotropy to detect in vivo stimulus-induced changes in chemoreceptor packing. *Methods Mol. Biol.* **1729**, 247–252 (2018).
52. J. S. Parkinson, S. E. Houts, Isolation and behavior of *Escherichia coli* deletion mutants lacking chemotaxis functions. *J. Bacteriol.* **151**, 106–113 (1982).
53. P. Mowery, J. B. Ostler, J. S. Parkinson, Different signaling roles of two conserved residues in the cytoplasmic hairpin tip of Tsr, the *Escherichia coli* serine chemoreceptor. *J. Bacteriol.* **190**, 8065–8074 (2008).
54. U. K. Laemmli, Cleavage of structural proteins during the assembly of the head of bacteriophage T4. *Nature* **227**, 680–685 (1970).
55. P. Ames, J. S. Parkinson, Constitutively signaling fragments of Tsr, the *Escherichia coli* serine chemoreceptor. *J. Bacteriol.* **176**, 6340–6348 (1994).
56. C. A. Schneider, W. S. Rasband, K. W. Eliceiri, NIH Image to ImageJ: 25 years of image analysis. *Nat. Methods* **9**, 671–675 (2012).
57. M. K. Slocum, J. S. Parkinson, Genetics of methyl-accepting chemotaxis proteins in *Escherichia coli*: Null phenotypes of the *tar* and *tap* genes. *J. Bacteriol.* **163**, 586–594 (1985).
58. A. Boyd, M. I. Simon, Multiple electrophoretic forms of methyl-accepting chemotaxis proteins generated by stimulus-elicited methylation in *Escherichia coli*. *J. Bacteriol.* **143**, 809–815 (1980).
59. G. E. Crooks, G. Hon, J. M. Chandonia, S. E. Brenner, WebLogo: A sequence logo generator. *Genome Res.* **14**, 1188–1190 (2004).
60. A. Pedetta, D. A. Massazza, M. K. Herrera Seitz, C. A. Studdert, Mutational replacements at the "glycine hinge" of the *Escherichia coli* chemoreceptor Tsr support a signaling role for the C-Helix residue. *Biochemistry* **56**, 3850–3862 (2017).
61. M. Hulko *et al.*, The HAMP domain structure implies helix rotation in transmembrane signaling. *Cell* **126**, 929–940 (2006).
62. Q. Zhou, P. Ames, J. S. Parkinson, Biphasic control logic of HAMP domain signalling in the *Escherichia coli* serine chemoreceptor. *Mol. Microbiol.* **80**, 596–611 (2011).